Published in final edited form as:
J Vasc Interv Radiol. 2012 April ; 23(4): . doi:10.1016/j.jvir.2011.12.017.

Effects of Near-Infrared Laser Irradiation of Biodegradable Microspheres Containing Hollow Gold Nanospheres and Paclitaxel Administered Intra-arterially in a Rabbit Liver Tumor Model

Sanjay Gupta, **R. Jason Stafford**, **Sanaz Javadi**, **Efe Ozkan**, **Joe E. Ensor**, **Kenneth C. Wright**, **Andrew M. Elliot**, **You Jian**, **Rita E. Serda**, **Katherine A. Dixon**, **Jennifer J. Miller**, **Sherry Klump**, **Michael J. Wallace**, and **Chun Li**
Departments of Diagnostic Radiology (S.G., S.J., E.O., K.W., K.D., J.M.), Imaging Physics (J.S., AE.), Experimental Diagnostic Imaging (Y.J., C.L.), Biostatistics (J.E.), and Veterinary Medicine & Surgery (S.K.), The University of Texas MD Anderson Cancer Center, 1515 Holcombe Blvd, Houston, TX., and Department of Nanomedicine (R.E.S.), The Methodist Hospital Research Institute, 6670 Bertner Ave, Houston, TX

Abstract

Purpose—To evaluate the effects of near-infrared (NIR) laser irradiation of microspheres (MS) containing hollow gold nanospheres (HAuNS) and paclitaxel (PTX) administered intra-arterially in an animal model.

Materials and Methods—For the ex-vivo experiments, VX2 tumor-bearing rabbits underwent hepatic artery (HA) administration of MS-HAuNS or MS. The animals were killed, the liver tumors were subjected to NIR irradiation, and temperature changes were estimated with magnetic resonance imaging. For the in-vivo study, VX2 tumor-bearing rabbits were randomized to 3 groups: MS-HAuNS-PTX-plus-NIR, MS-HAuNS-PTX, and saline-plus-NIR. Laser irradiation was delivered at 1 hour and at 3 days after HA administration of saline or MS-HAuNS-PTX. Animals were euthanized and tumors were analyzed for necrosis and apoptosis. Plasma samples were collected from the MS-HAuNS-PTX-plus-NIR animals for PTX analysis.

Results—Ex-vivo experiments showed intratumoral heating in animals that received MS-HAuNS but no temperature change in animals that received MS. Animals treated with MS-HAuNS-PTX-plus-NIR showed a transient increase in plasma PTX levels after each NIR irradiation and significantly greater tumor necrosis than did those that received MS-HAuNS-PTX or saline-plus-NIR (44.9% vs. 13.8% or 23.7%, respectively; $P < .0001$). The mean apoptotic index in the MS-HAuNS-PTX-NIR group (5.01 ± 1.66) was significantly higher than that in the MS-HAuNS-PTX (2.99 ± 0.97) or saline-plus-NIR (1.96 ± 0.40) groups ($P = .0013$).

Conclusions—NIR laser irradiation after MS-HAuNS-PTX administration results in intratumoral heating and increases the efficacy of treatment. Further studies are required to evaluate the optimal laser settings to maximize therapeutic efficacy.

Address correspondence to Sanjay Gupta, MD, Department of Diagnostic Radiology, Unit 1471, The University of Texas MD Anderson Cancer Center, 1515 Holcombe Blvd, Houston, TX 77030. Telephone: (713) 794-4855; fax: (713) 792-4098; sgupta@mdanderson.org.

Gold nanostructures, such as gold nanoshells, hollow gold nanospheres (HAuNS), and gold nanorods, have been used for photothermal ablation of tumors. These nanoparticles exhibit a strong optical extinction at near-infrared (NIR) wavelengths (700–850 nm) because of the localized surface plasmon resonance of their free electrons upon excitation by an electromagnetic field (1, 2). Absorption of NIR light results in resonance and the transfer of thermal energy to the surrounding medium or tissue.

Recent progress in the field of nanotechnology has led to the identification of various inorganic nanoparticles such as iron oxide nanoparticles, carbon nanohorns, carbon nanotubes, and gold nanoparticles as attractive vehicles for drug delivery. Hollow gold nanospheres (HAuNS) are a novel class of gold nanoparticles having plasmon absorption in the NIR region that display a strong photothermal coupling property suitable for photothermal ablation therapy (3, 4). The unique combination of small size (30–50 nm in diameter), absence of a silica core, spherical shape, strong and tunable (520–950 nm) absorption band, and the lack of need for cytotoxic surfactant to stabilize other gold nanoparticles suggest that HAuNS may be useful for in vivo molecular therapy (3, 4).

Use of external stimuli such as magnetization and light to trigger drug delivery from nanoparticles is an attractive strategy because it can increase intratumoral drug concentration, decrease systemic toxicity, and allow temporal and spatial control over drug release. NIR light–triggered drug release is a promising approach for the spatiotemporal control of drug delivery. NIR light is already being used in the clinic for molecular imaging and for cancer ablation therapy. Bikram et al. (5) demonstrated temperature- modulated drug delivery from SiO_2/Au nanoshells embedded within temperature-sensitive hydrogels. Bedard et al. (6) showed the NIR-triggered release of dextran from multilayered polyelectrolyte microshells containing aggregates of colloidal gold. Wu et al. (7) used a femtosecond-pulsed laser to trigger release of a dye molecule from liposomes containing HAuNS. However, the release of therapeutically significant anticancer drugs from these systems in a clinically relevant setting has not been investigated.

In an earlier study, we fabricated biodegradable, biocompatible poly(lactide-co-glycolide) (PLGA) copolymer-based microspheres (MS) containing paclitaxel (PTX) and HAuNS as the photothermal coupling agent, and evaluated the drug-release properties, in vitro cytotoxicity, and in vivo antitumor activity of these MS mediated by NIR light (8). The results showed that the release of PTX from the MS is readily controlled by the output power of the NIR laser, duration of irradiation, treatment frequency, and concentration of HAuNS embedded inside the MS. In vitro, cancer cells incubated with PTX and HAuNS-loaded MS (MS-HAuNS-PTX) and irradiated with NIR light displayed significantly greater cytotoxic effects than did cells incubated with the MS alone or cells irradiated with NIR light alone. Treatment of subcutaneously implanted human U87 gliomas and MDA-MB-231 mammary tumor xenografts in nude mice with intratumoral injections of MS-HAuNS-PTX followed by surface NIR irradiation has resulted in significantly delayed tumor growth compared with the growth of tumors treated with HAuNS-loaded MS (no PTX) plus NIR irradiation or with MS-HAuNS-PTX alone. The data supported the feasibility of a therapeutic approach in which NIR light is used for simultaneous modulation of drug release and induction of photothermal cell killing to maximize therapeutic effect. However, in clinical practice, most tumors are located deep inside the body and may not be amenable to direct intratumoral injection of particles or treatment by surface NIR irradiation. Hence, we conducted this experiment to evaluate the feasibility and efficacy of using a percutaneously inserted laser fiber for NIR laser irradiation of MS-HAuNS-PTX administered intra-arterially in a rabbit liver tumor model.

Materials and Methods

Synthesis of HAuNS

Polyethylene glycol (PEG)-coated HAuNS were synthesized using a previously reported method (3, 4). Cobalt nanoparticles were first synthesized by reducing cobalt chloride (1 mL, 0.4 mol/L; Fisher Scientific, Pittsburgh, PA) with sodium borohydride (4.5 mL, 1 mol/L; Fisher Scientific) in deionized water containing 2.8 mL of sodium citrate (0.1 mol/L; Fisher Scientific). HAuNS were obtained by adding chloroauric acid (Fisher Scientific) into the solution containing cobalt nanoparticles.

For PEG coating, HAuNS (5.0×10^{12} particles/mL) were added to argon-purged aqueous solution containing methoxy-polyethylene glycol-SH (molecular weight 5,000; Nektar Therapeutics, Huntsville, AL) with various concentrations. The reaction was allowed to proceed overnight at room temperature. For purification, the reaction mixture was centrifuged at 14,000 rpm for 20 minutes, and the resulting pellet was resuspended with deionized water. The process was repeated twice to remove unreacted PEG molecules.

MS Preparation and PTX Loading

A modified water-in-oil-in-water (W1/O/W2) double-emulsion solvent evaporation method was used to prepare PLGA MS containing both HAuNS and PTX (MS-HAuNS-PTX). The first emulsion was formed by mixing an aqueous solution (0.08 mL) containing HAuNS ($\sim 1 \times 10^{12}$ particles) with dichloromethane (0.8 mL) coining PLGA (240 mg; DURECT Corp., Cupertino, CA) and PTX (24 mg; Yunnan Hande Bio-Tech Co., Ltd., Houston, TX), which was then injected into an aqueous solution of 2% polyvinyl alcohol (8.0 mL; Polysciences, Inc., Warrington, PA) serving as the external aqueous phase. W1/O/W2 emulsion was achieved by using a POLYTRON PT-MR 3000 benchtop homogenizer from Kinematica AG (Lucerne, Switzerland) at 15,000 rpm. The MS were formed after the organic solvent was completely evaporated, washed three times with water, and freeze-dried. MS-HAuNS were prepared similarly but without the addition of PTX.

PTX Loading Analysis

The amount of PTX in the MS was determined by an Agilent 1100 Series high-performance liquid chromatography (Santa Clara, CA). PTX loading was expressed as PTX content in dry MS (w/w).

Animal Care

The Institutional Animal Care and Use Committee (IACUC) approved the animal experiments. The rabbits were maintained in facilities approved by the Association for Assessment and Accreditation of Laboratory Animal Care and in accordance with current U.S. Department of Agriculture, Department of Health and Human Services, and National Institutes of Health Regulations and Standards.

Tumor Inoculation

Each rabbit was sedated with an intramuscular injection of buprenorphine (0.15 mg; Bedford Laboratories, Bedford, OH), and anesthesia was induced with 5% isoflurane/oxygen (1.5 L/min) administered via mask and maintained with 3%–5% isoflurane/oxygen (1.5 L/min). Enrofloxacin antibiotic (Baytril; Bayer Corporation, Agriculture Division, Animal Health, Shawnee Mission, KS) was given intramuscularly at a dose of 5.0 mg/kg. The abdomen was shaved and prepared for aseptic surgery. A small midline incision was made, and the left lateral lobe of the liver was exteriorized and inoculated at a single site with 0.3 mL of freshly harvested and prepared VX2 tumor fragments. The fragments were placed in the

liver through an 18-gauge needle attached to a 1-mL syringe. After hepatic inoculation, the abdomen was closed in layers, and the animal was kept warm and monitored until it recovered from anesthesia. The tumors were allowed to grow in the rabbits' livers for 14–16 days before treatment and reached a diameter of approximately 1–1.5 cm.

Ex Vivo Experiments

Ex-vivo experiments were performed in two New Zealand white rabbits fourteen days after liver VX2 tumor implantation. Each rabbit was anesthetized with a 150-mg intramuscular injection of ketamine (Fort Dodge Animal Health, Fort Dodge, IA) and 10 mg of acepromazine (Vedco, Inc., Saint Joseph, MO). A 22-gauge intravenous catheter (Insyle™ Autogard™ Winged; Becton Dickinson Therapy Systems Inc., Sandy, UT) was placed in a marginal ear vein, and anesthesia was maintained with use of intravenous injections of 25 mg/mL of thiopental sodium (pentothal; Hospira, Inc., Lake Forest, IL) given to effect. The right groin was shaved and prepared for aseptic surgery. The right femoral artery was isolated via a cut down, a 4.0 Fr introducer sheath (Cook Inc., Bloomington, IN) was placed in the artery through a small arteriotomy, and heparin sodium (100 IU/kg) was administered. A 2.8 Fr microcatheter (EmboCath Plus; BioSphere Medical, Rockland, MA) was inserted through the sheath in the femoral artery. With the help of a 0.014-in. pre-shaped hydrophilic guidewire (Transend; Boston Scientific, Miami, FL), the microcatheter was advanced up the aorta and manipulated into the celiac axis under fluoroscopic monitoring. A digital subtraction arteriogram was performed to document the location and size of the tumor and to delineate its blood supply. The catheter was then manipulated into the proper hepatic artery and positioned distal to the origin of the gastroduodenal artery. Blood flow around the catheter and the absence of arterial spasm were verified by hand-injection of the contrast/saline mixture. One animal underwent hepatic arterial (HA) administration of MS-HAuNS suspended in 1 mL of a solution containing 0.5 mL of nonionic contrast medium (Visipaque 320; GE Healthcare, Inc., Princeton, NJ) and 0.5 mL of saline; the other animal underwent HA administration of plain MS dissolved in 1 mL of the same solution. The animals were euthanized 1 hour later with an overdose of Beuthanasia-D (1.0 mL/10 lb), and their livers were removed en bloc and mounted in a saline bath (maintained at 33°C) in order to conduct controlled exposure experiments in the tumors and to observe the spatiotemporal temperature changes.

An 808-nm NIR 600-μm-diameter laser fiber (BioTex, Inc., Houston, TX) with a 1-cm-long diffusing tip was inserted into the liver tumor under ultrasound guidance, and laser irradiation was performed at 1.5 W with use of a Diomed 15 laser system (New York, NY). Magnetic resonance temperature imaging was performed in a 1.5T clinical scanner (Excite HD, GE Healthcare Technologies, Waukesha, WI) using a quadrature transmit and receive knee coil. A multi-echo gradient-recalled echo sequence using a 12 echo train with 3.4-ms spacing was used for fast high-resolution chemical shift imaging in order to measure temperature-dependent changes in the proton resonance frequency shift (9). Acquisition parameters were as follows: repetition time (TR) = 40 ms, echo time (TE) = 2 ms, flip angle = 30°, acquisition matrix = 128 × 128 (zero padded to 256 × 256), field of view = 180 mm, slice thickness = 4 mm, and receiver bandwidth = 244 Hz/pixel. Temperature changes were estimated from the 12-echo chemical shift imaging acquisition by using an iterative autoregressive moving average algorithm (9). A temperature sensitivity coefficient of –0.01 ppm/°C was used. Background drift in the sample was corrected for by subtracting the mean from an adjacent region of interest outside the region of heating. All processing and analysis of MR temperature images was performed off-line with use of in-house algorithms implemented in MATLAB (MathWorks, Natick, MA).

In vivo experiments

Hepatic VX2 tumor implantation was performed in 17 New Zealand white rabbits (3.5–4.2 kg). The experimental animals were divided into three treatment groups: MS-HAuNS-PTX-plus-NIR group (n = 7; dose: 4 mg PTX in 40 mg MS for each animal), MS-HAuNS-PTX group (n = 5; dose: 4 mg PTX in 40 mg MS for each animal), and saline-plus-NIR group (n = 5). Animals in the MS-HAuNS-PTX-NIR and MS-HAuNS-PTX groups underwent HA administration of MS-HAuNS-PTX suspended in 1 mL of a solution containing 0.5 mL of nonionic contrast medium (Visipaque 320; GE Healthcare, Inc.) and 0.5 mL of saline, whereas the animals in the saline-plus-NIR group underwent HA administration of 1 mL of a solution containing 0.5 mL of nonionic contrast medium (Visipaque 320) and 0.5 mL of saline. Using the technique described earlier in the ex-vivo experiment section, each rabbit was anesthetized, and hepatic arterial catheterization and administration of respective materials in each treatment group was performed under continuous fluoroscopic monitoring to avoid any reflux into the gastroduodenal or gastric arteries. The MS-HAuNS-PTX-plus-NIR and saline-plus-NIR groups were treated with NIR laser at 1 hour and at 3 days after intra-arterial administration. Animals were maintained on intravenous anesthesia with thiopental sodium and laser stimulation was performed at 1 hour after HA administration of MS or saline. For the second laser stimulation experiment three days after HA administration of MS or saline, animals were anesthetized with isoflurane (5%)/oxygen (1.5 L/min) administered via mask. An endotracheal tube was placed and anesthesia maintained with isoflurane (3%–4%)/oxygen (1.5 L/min). With use of ultrasound guidance, an 18-gauge guide needle was placed percutaneously into the tumor through which an 808 nm 600-μm-diameter laser fiber (BioTex, Inc., Houston, TX) with a 1-cm-long diffusing tip was introduced. A NIR diode laser system (Diomed 15; New York, NY) was used for laser stimulation at 1.5 W for 3 minutes.

To demonstrate the proof of concept in an in vivo setting, in one of the animals in the MS-HAuNS-PTX-plus-NIR group, MR temperature imaging was performed at the 1-hr NIR irradiation to assess the intratumoral temperatures during NIR irradiation. Gentle pressure via use of a strap to restrict respiratory breathing in the area was applied to the abdomen of the animal during imaging to minimize liver motion. In this case, a slightly faster (2.8 sec per image) MR temperature imaging sequence was used with single gradient-echo acquisition (TR/TE= 22 ms/10 ms, flip angle = 20°, field of view = 120 × 120 mm, acquisition matrix = 128 × 128, slice thickness = 6 mm, and receiver bandwidth = 156 Hz/pixel) to minimize the potential for intra-scan motion artifacts in the images. As before, complex phase-subtract and temperature-dependent resonance frequency (–0.01 ppm/°C) were used to estimate temperature changes in the tissue.

Histological Analysis

All animals were euthanized 7 days after HA administration of MS or saline with an overdose of Beuthanasia-D (1.0 mL/10 lb). Tumors were excised at necropsy and placed in 10% neutral buffered formalin. The fixed tissues were then embedded in paraffin blocks from which 4-μm sections were cut and stained with hematoxylin and eosin for necrosis evaluation, and TUNEL staining was performed for apoptosis assessment.

For necrosis evaluation, tissue glass slides were digitized via whole-slide scanning with a 20× objective by using the Aperio ScanScope CS system (Aperio Technologies, Vista, CA). A veterinary pathologist examined the specimens under light microscopy. The necrosis percentage was determined by the ratio of necrosis to intact tumor in each slide, and the overall necrosis in each group was determined by average necrosis in that group.

For apoptosis evaluation, TUNEL staining of tissue slides was performed with a TACS® insito apoptosis detection kit (Trevigen, Inc, Gaithersburg, MD). Apoptosis was scored by microscopic examination at 40× magnification. Five fields of non-necrotic areas were randomly selected in each histological section; in each field, the number of apoptotic nuclei were recorded as numbers per 100 nuclei scored (500), and the results were expressed as a percentage for each slide. Two observers determined that the apoptotic index and mean apoptotic index was obtained.

PTX Analysis

Blood samples were collected from all MS-HAuNS-PTX-plus-NIR group animals. On day 1, blood was collected via a catheter inserted in an ear vein of the animals just before administration of MS-HAuNS-PTX, at 10 and 50 minutes after administration, and at 10 and 30 minutes after laser irradiation. Three days later, blood samples were collected at 10 minutes before and at 10 and 30 minutes after the second laser irradiation. Blood samples were also collected just before euthanization of the animals. The PTX levels in these blood samples were analyzed by using liquid chromatography-mass spectrometry.

Tissue Preparation for Scanning Electron Microscopy

For tissue scanning electron microscopy (SEM), tissues were processed according to the previously described techniques (10). Tissues were embedded in 3% agarose; 100-μm-thick tissue sections were cut with use of either a Krumdieck MD-4000 Tissue Slicer (Alabama Research & Development, Munford, AL). Sections were stained with 0.2 M cacodylate-buffered 2% tannic acid and 0.1 M cacodylate-buffered 2% osmium tetroxide, and then dehydrated in increasing concentrations of ethanol followed by infiltration with 100% t-butanol for 30 minutes. Samples were dried in a dessicator and then mounted on SEM sample stubs using carbon adhesive tape. Sections were then sputter-coated with 10 nm of gold and imaged with an Quanta 400 FEG SEM (FEI, Hillsboro, OR).

Statistical Analysis

A one-way ANOVA F-test was used to evaluate the mean necrosis percentage and apoptotic index among the three groups. The Tukey-Kramer multiple comparison procedure was used to protect the familywise/experimentwise error while conducting multiple comparisons. $P < .05$ was considered statistically significant.

Results

MR Temperature Imaging

Ex vivo experiments in the liver in which MS-HAuNS had been administered showed measurable temperature increase on MR imaging (Fig 1). Maximum estimated temperature changes were 8.6°C at 1 minute, 12.4°C at 3 minutes, and 13.9°C at 5 minutes at an output power of 1.5 W; these temperatures were observed close to the position of the laser fiber. The standard deviation in the temperature across the tumor region was 0.03°C before the laser was turned on. The mean and standard deviation of temperature change along the borders of the lesion was 4.0°C ± 1.7°C, 7.4°C ± 2.3°C, and 8.5°C ± 2.6°C at the 1-, 3-, and 5-minute time points, respectively. Similar temperature changes were noted in the in vivo experiment performed in one animal in the MS-HAuNS-PTX-plus-NIR group. The estimated maximum temperature change in the tumor was 18°C, whereas the mean and standard deviation was 15.4°C ± 2.1°C (Fig 2). Ex vivo experiments in the liver in which plain MS without nanoshells were injected did not result in any observable temperature change.

Delivery of MS into VX2 Tumor

Hematoxylin and eosin staining preparations showed variable degrees of tumor necrosis in the VX2 tumors. The MS-HAuNS were present in the tumoral and peritumoral vessels as well as in the interstitial tissues. The MS-HAuNS appeared as rounded structures and ranged in size from 20 to 100 microns (Fig 3a). Scanning electron microscopy confirmed the presence of MS-HAuNS in the tumor vessel (Fig 3b).

PTX Release

Plasma PTX levels in the MS-HAuNS-PTX-plus-NIR group from the time of HA administration until necropsy are shown in Figure 4. PTX levels peaked immediately after HA administration followed by a gradual decline. A transient increase in plasma PTX levels was noted after each NIR irradiation, especially after the NIR irradiation on day 3 of the experiment. However, these differences between PTX levels before and after each laser treatment did not reach statistical significance.

Tumor Necrosis Quantification

The extent of necrosis in each group of rabbits is summarized in Figure 5a. MS-HAuNS-PTX-plus-NIR induced significantly more tumor necrosis (44.9% ± 15.4%) than did MS-HAuNS-PTX alone (13.8% ± 6.9%; $P = .0008$) or saline-plus-NIR (23.7% ± 5.2%; $P = .0147$). The difference in the mean tumor necrosis between the MS-HAuNS-PTX and saline-plus-NIR groups was not statistically significant ($P = .3608$).

Tumor Apoptosis Quantificatio

TUNEL assay showed that the mean apoptotic index (Fig 5b) in the MS-HAuNS-PTX-plus-NIR group (5.01 ± 1.66) was significantly higher than in the MS-HAuNS-PTX alone (2.99 ± 0.97; $P = .0156$) or saline-plus-NIR (1.96 ± 0.40; $P = .0013$) group. The difference in the mean apoptotic index between the MS-HAuNS-PTX alone and saline-plus-NIR groups was not statistically significant ($P = .3322$).

Discussion

In this study, we investigated the potential clinical use of NIR-radiation–triggered photothermal effect to modulate drug delivery from temperature-sensitive PLGA MS containing optically active gold nanoshells and an anticancer agent. Our data show that NIR laser irradiation mediated via a percutaneously placed fiber after HA administration of MS-HAuNS results in intratumoral heating in a rabbit VX2 liver tumor model, triggers release of PTX from MS-HAuNS-PTX and increases the efficacy of treatment after IA delivery of MS-HAuNS-PTX in liver tumors. The enhanced antitumor activity in tumors treated with MS-HAuNS-PTX-plus- NIR irradiation is likely a result of both the cytotoxic effect of PTX and the photothermal effect mediated by HAuNS.

The ability of nanoparticles to convert NIR laser radiation to heat has been demonstrated in many recent studies (1, 2). In our ex vivo experiments, heating was noted only in liver tumors containing MS-HAuNS, not in liver tumors containing plain MS, clearly demonstrating that at the laser power settings used, local heating was associated with photothermal interaction between the gold nanoshells and NIR, not from direct heating from NIR irradiation. Spatiotemporal thermal profiles observed in the current experiment are consistent with the results from earlier studies using gold nanoshells embedded in gel phantoms or ex vivo canine livers (11-13). Maximum temperature changes were noted in the immediate vicinity of the laser fiber and gradually decreased with increasing distances from the fiber. Since the nanoshells were injected intra-arterially and randomly distributed in the

tumors, this peripheral fall-off in heating was likely not related to HAuNS concentration but was more likely secondary to reduced NIR intensities due to both scattering from tissue and absorption from HAuNS. Although heating was noted at 6–8 mm from the laser fiber, greater depths and higher temperatures can be potentially achieved with higher laser powers or extended irradiation. The maximum achievable temperatures and maximum depth at which temperature changes are observed will also vary, depending on the tissue or tumor type because attenuation properties of tissues differ.

Temporal and spatial controlled release has the potential of increasing drug delivery to the tumor and allowing prolonged exposure of the tumor to the chemotherapeutic drug, thereby increasing therapeutic efficacy. NIR radiation-induced drug release from nanoshells or nanoshell-containing hydrogels has been shown in a number of in vitro studies (5-7). Our earlier in vitro experiments using MS-HAuNS-PTX had shown that rapid, repetitive PTX release occurred upon irradiation with NIR light (808 nm), whereas PTX release was insignificant when the NIR light was switched off (8). In the present study, pharmacokinetic analysis showed that PTX levels peaked immediately after HA administration and then gradually declined. This initial rapid release of PTX could be attributed to the burst effect of PTX-loaded MS. Such a burst release effect was not observed previously when MS-HAuNS-PTX was incubated in phosphate-buffered saline solution (8). It is likely that the presence of blood accelerated the release of PTX from MS-HAuNS-PTX. The burst effect may be reduced by optimizing the MS formulation and by increasing the efficiency of PTX loading. It was also noted that the plasma level of PTX was maintained at least 7 days in rabbits that received HA administration of MS-HAuNS-PTX; this sustained release of PTX from the MS should enhance the antitumor activity of PTX against hepatocellular carcinoma or metastases in the liver. Although the observed pharmacokinetic profile does not provide definite evidence of laser-stimulated release of PTX from the microspheres, the transient increase in plasma PTX levels noted after each NIR irradiation indirectly suggests that NIR irradiation plays some role in augmenting PTX release. Further studies should be designed to better understand the NIR laser-mediated intratumoral drug release from the MS- HAuNS formulations in an in-vivo setting.

We used PTX in this study because it has been shown to be an effective mitotic inhibitor and apoptosis inducer in tumor cells and is a widely used agent to treat a variety of human cancers (14, 15). Paclitaxel has also been shown to have cytotoxic activity against human hepatocellular cancer cell lines (16, 17). However, other anticancer agents that are commonly used for intra-arterial regional treatment, such as doxorubicin, can easily be incorporated into the MS-HAuNS formulation used in our study.

In an in vitro experiment involving mouse melanoma B16F10 cells, Wu et al. (18) reported the use of multifunctional hybrid nanogels (constructed by coating the Ag-Au bimetallic nanoparticle core with a thermoresponsive nonlinear PEG-based hydrogel as a shell) loaded with the anticancer drug temozolomide (for combined local chemotherapy) and combined with photothermal treatment using external NIR radiation (18). Although other investigators have reported a similar concept of incorporating nanoparticles in biodegradable hydrogels or liposomes and using external NIR radiation for mediating drug release, to our knowledge, the use of these nanosystems in a clinically relevant large animal model has not been investigated (5, 7).

Our study shows the multifunctional potential of encapsulating gold nanoshells into biodegradable MS. Microspheres (20-100 micron) act as embolic agents and lodge in the intratumoral and peritumoral vessels after HA administration. Findings on both light and scanning electron microscopy confirmed the presence of MS in the intratumoral and peritumoral vessels. Encapsulation of HAuNS into the MS does not interfere with the

photothermal sensitivity of nanoshells, as shown by the temperature changes observed in the ex vivo experiments of the current study as well as in in vitro experiments from a previous study (8); hence these nanoshell-containing MS can be used for mediating photothermal ablation of tumors. In addition, cytotoxic drugs can be loaded into the MS, allowing local intratumoral delivery of chemotherapeutic agents. Although not definitely proven in the current study, results of our earlier in-vitro study suggest that NIR laser radiation-mediated nanoshell heating can be used to potentiate release of the drug from the thermoresponsive MS.

In this study, antitumor activity was assessed by using necrosis percentage and apoptosis rates. We observed statistically significant increases in necrosis and apoptosis percentage in the MS-HAuNS-PTX-plus-NIR treatment group compared with the other two treatment groups. These findings suggest that HA infusion of MS-HAuNS-PTX followed by NIR irradiation using a percutaneously placed laser fiber may produce prominent antitumor effects. The enhanced antitumor activity in tumors treated with MS-HAuNS-PTX and NIR irradiation is likely a result of both the cytotoxic effect of the PTX release and the photothermal effect mediated by HAuNS. The results of our study are in keeping with earlier studies that have suggested that a combination of thermal ablation and local delivery of a chemotherapeutic agent can result in better tumor control than does treatment with a single method (19-21). However, substantial viable tumor was identified even in the MS-HAuNS-PTX-plus-NIR treatment group in the present study. This finding may be associated with a number of factors. For example, it is possible that the NIR effect was limited to the immediate vicinity of the fiber and did not extend into the periphery of the tumor; this can potentially be corrected by increasing the NIR power or by placing additional fibers in the tumor. Further studies are required for optimization of laser fiber placement and NIR radiation settings to achieve better tumor control.

Our study has several limitations. First, the temperature changes were measured in ex vivo livers, but the presence of blood circulation in vivo may alter the temperature changes achieved after laser stimulation. We did observe similar temperature changes on in vivo MR temperature imaging performed in one animal. However, further in vivo MR thermal mapping studies in a larger number of animals is required to assess the intratumoral and peritumoral thermal profile after NIR irradiation. Second, we did not measure the intratumoral PTX concentrations or distribution after NIR stimulation; hence, we were not able to assess the drug concentrations in different parts of the tumor. Third, since we did not mark the position of the laser fiber, we could not quantify the treatment effect as a function of distance from the laser fiber. Fourth, the experimental parameters that we used, such as MS-HAuNS concentrations and the power, duration, and frequency of the laser, were based on previous experience. Therefore, the study design did not allow determination of optimal treatment conditions, including the optimal nanoparticle concentration and laser settings to induce maximal photothermal effect, drug release, and cell killing.

In conclusion, this preliminary feasibility study demonstrated that NIR irradiation, mediated via percutaneously placed intratumoral laser fibers, can be used for local intratumoral heating and has the potential to mediate drug release from intra-arterially injected MS-HAuNS-PTX. Furthermore, this therapeutic approach enhanced tumor killing in a rabbit liver tumor model. Future studies will focus on improving drug loading and NIR radiation settings to maximize antitumor effects.

Acknowledgments

We would like to thank the Cancer Center Support Grant Mutant Mouse Pathology Service for their technical assistance in the slide scanning procedure.

This material was presented at an SIR Annual Meeting, 2011. This research was supported in part by grants from the Hogg Foundation and John S. Dunn Research Foundation, and by NIH Cancer Center Support Grant CA016672 awarded by the National Cancer Institute.

References

1. El-Sayed IH, Huang X, El-Sayed MA. Selective laser photo-thermal therapy of epithelial carcinoma using anti-EGFR antibody conjugated gold nanoparticles. Cancer Lett. 2006; 239:129–135. [PubMed: 16198049]
2. O'Neal DP, Hirsch LR, Halas NJ, Payne JD, West JL. Photo-thermal tumor ablation in mice using near infrared-absorbing nanoparticles. Cancer Lett. 2004; 209:171–176. [PubMed: 15159019]
3. Lu W, Xiong C, Zhang G, et al. Targeted photothermal ablation of murine melanomas with melanocyte-stimulating hormone analog-conjugated hollow gold nanospheres. Clin Cancer Res. 2009; 15:876–886. [PubMed: 19188158]
4. Melancon MP, Lu W, Yang Z, et al. In vitro and in vivo targeting of hollow gold nanoshells directed at epidermal growth factor receptor for photothermal ablation therapy. Mol Cancer Ther. 2008; 7:1730–1739. [PubMed: 18566244]
5. Bikram M, Gobin AM, Whitmire RE, West JL. Temperature-sensitive hydrogels with SiO2-Au nanoshells for controlled drug delivery. J Control Release. 2007; 123:219–227. [PubMed: 17920154]
6. Bedard MF, Braun D, Sukhorukov GB, Skirtach AG. Toward self-assembly of nanoparticles on polymeric microshells: near-IR release and permeability. ACS Nano. 2008; 2:1807–1816. [PubMed: 19206419]
7. Wu G, Mikhailovsky A, Khant HA, Fu C, Chiu W, Zasadzinski JA. Remotely triggered liposome release by near-infrared light absorption via hollow gold nanoshells. J Am Chem Soc. 2008; 130:8175–8177. [PubMed: 18543914]
8. You J, Shao R, Wei X, Gupta S, Li C. Near-infrared light triggers release of Paclitaxel from biodegradable microspheres: photothermal effect and enhanced antitumor activity. Small. 6:1022–1031. [PubMed: 20394071]
9. Taylor BA, Hwang KP, Elliott AM, Shetty A, Hazle JD, Stafford RJ. Dynamic chemical shift imaging for image-guided thermal therapy: analysis of feasibility and potential. Med Phys. 2008; 35:793–803. [PubMed: 18383702]
10. Hashizume H, Baluk P, Morikawa S, et al. Openings between defective endothelial cells explain tumor vessel leakiness. Am J Pathol. 2000; 156:1363–1380. [PubMed: 10751361]
11. Elliott A, Schwartz J, Wang J, Shetty A, Hazle J, Stafford JR. Analytical solution to heat equation with magnetic resonance experimental verification for nanoshell enhanced thermal therapy. Lasers Surg Med. 2008; 40:660–665. [PubMed: 18951423]
12. Elliott AM, Shetty AM, Wang J, Hazle JD, Jason Stafford R. Use of gold nanoshells to constrain and enhance laser thermal therapy of metastatic liver tumours. Int J Hyperthermia. 26:434–440. [PubMed: 20597626]
13. Hirsch LR, Stafford RJ, Bankson JA, et al. Nanoshell-mediated near-infrared thermal therapy of tumors under magnetic resonance guidance. Proc Natl Acad Sci U S A. 2003; 100:13549–13554. [PubMed: 14597719]
14. Milross CG, Mason KA, Hunter NR, Chung WK, Peters LJ, Milas L. Relationship of mitotic arrest and apoptosis to antitumor effect of paclitaxel. J Natl Cancer Inst. 1996; 88:1308–1314. [PubMed: 8797771]
15. Xi G, Hu X, Wu B, et al. Autophagy inhibition promotes paclitaxel-induced apoptosis in cancer cells. Cancer Lett. 307:141–148. [PubMed: 21511395]
16. Gagandeep S, Novikoff PM, Ott M, Gupta S. Paclitaxel shows cytotoxic activity in human hepatocellular carcinoma cell lines. Cancer Lett. 1999; 136:109–118. [PubMed: 10211948]
17. Jin C, Li H, He Y, et al. Combination chemotherapy of doxorubicin and paclitaxel for hepatocellular carcinoma in vitro and in vivo. J Cancer Res Clin Oncol. 136:267–274. [PubMed: 19693537]

18. Wu W, Shen J, Banerjee P, Zhou S. Core-shell hybrid nanogels for integration of optical temperature-sensing, targeted tumor cell imaging, and combined chemo-photothermal treatment. Biomaterials. 31:7555–7566. [PubMed: 20643481]

19. Weinberg BD, Ai H, Blanco E, Anderson JM, Gao J. Antitumor efficacy and local distribution of doxorubicin via intratumoral delivery from polymer millirods. J Biomed Mater Res A. 2007; 81:161–170. [PubMed: 17120197]

20. Weinberg BD, Blanco E, Gao J. Polymer implants for intratumoral drug delivery and cancer therapy. J Pharm Sci. 2008; 97:1681–1702. [PubMed: 17847077]

21. Weinberg BD, Blanco E, Lempka SF, Anderson JM, Exner AA, Gao J. Combined radiofrequency ablation and doxorubicin-eluting polymer implants for liver cancer treatment. J Biomed Mater Res A. 2007; 81:205–213. [PubMed: 17120205]

Figure 1a

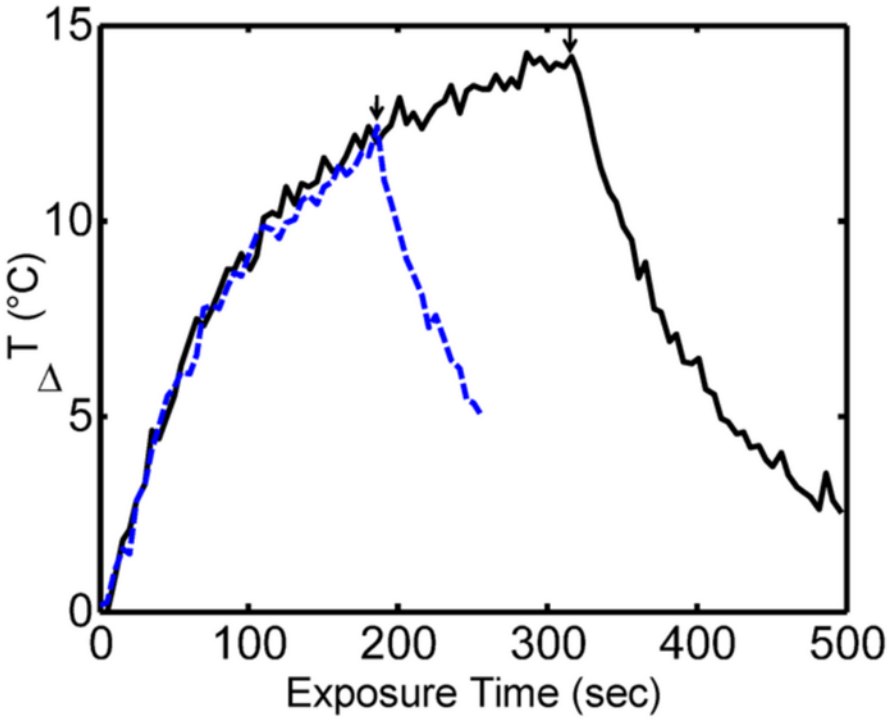

Figure 1b

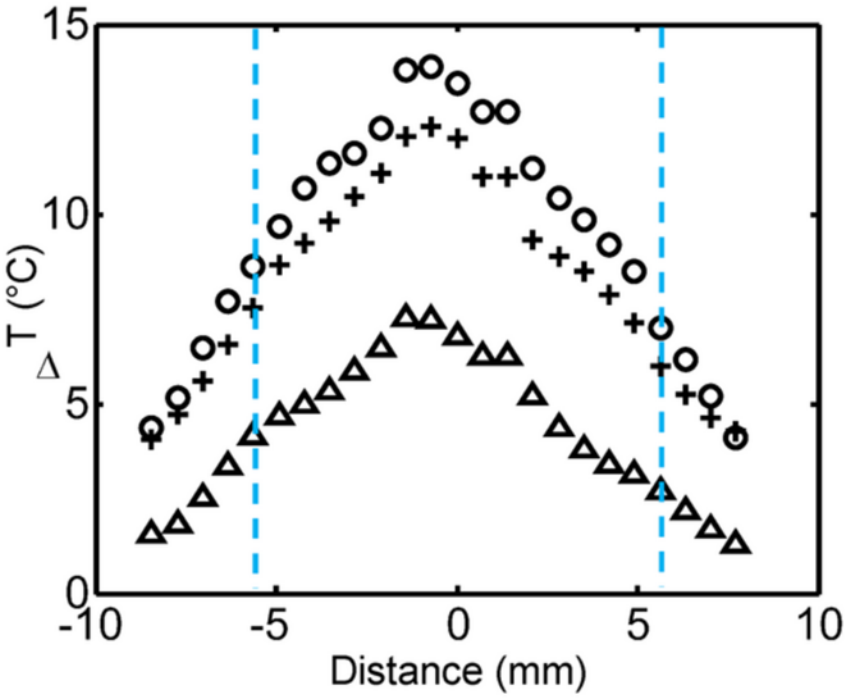

Figure 1c

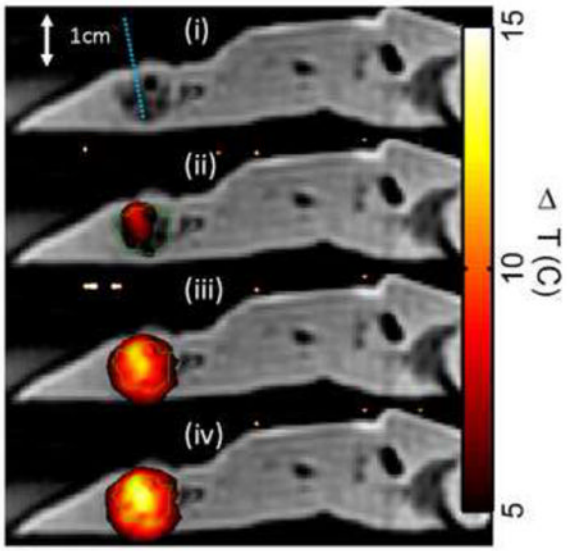

Figure 1.

Ex vivo MR temperature imaging. **(a)** The estimated maximum change in temperature as measured by proton resonance frequency shift over time for a 180-sec (dashed) and a 300-sec (solid) exposure of 1.5 W at 808 nm. **(b)** Spatial profiles orthogonal to the laser fiber for 60 sec (triangle), 180 sec (+), and 300 sec (o) exposure times are shown versus the approximate tumor boundaries (dashed). **(c)** The approximate location of the laser fiber in the tumor (dashed line) is shown on the magnitude image of the fast chemical shift imaging acquisition (i). An overlay of the temperature change (5°C–15°C) as measured by proton resonance frequency for 60-sec (ii), 180-sec (iii), and 300-sec (iv) exposures of 1.5 W at 808 nm with an outline of the approximate tumor boundaries (green) shown for reference.

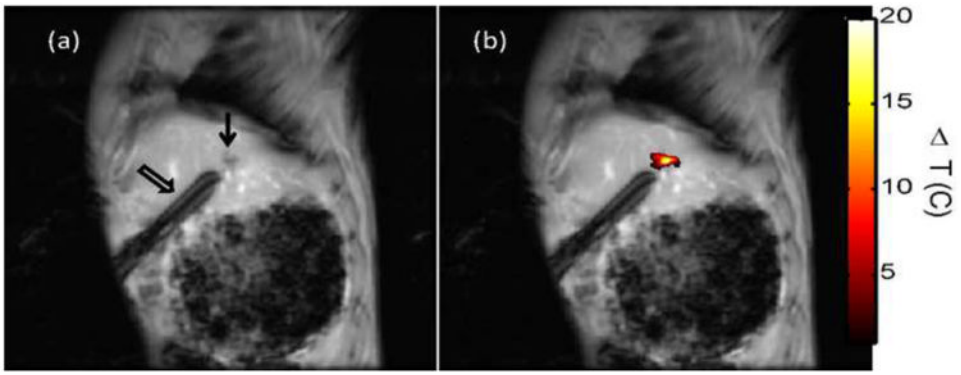

Figure 2.
In vivo MR temperature imaging. Magnetic resonance (MR) temperature imaging of laser exposure (1.5 W for 180 sec) of VX2 in the liver of rabbits injected with MS-HAuNS-PTX. Sagittal MR image **(a)** shows the liver VX2 tumor (arrow) and the laser fiber inserted through a guide cannula (open arrow), whereas **(b)** shows the MR temperature imaging–estimated maximum temperature rise at the end of the exposure overlaid on the image.

Figure 3a

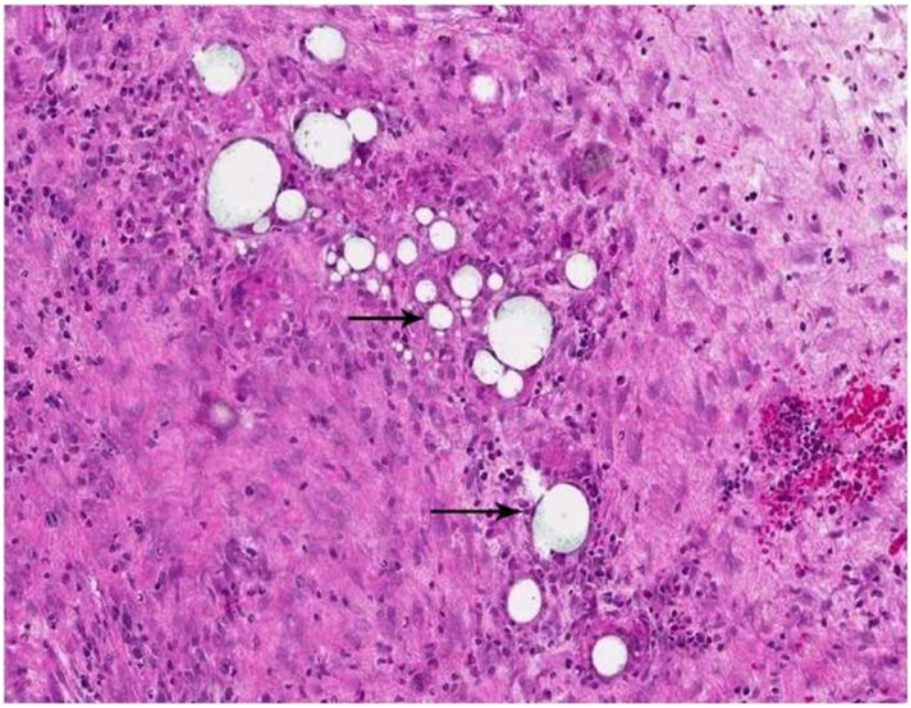

Figure 3b

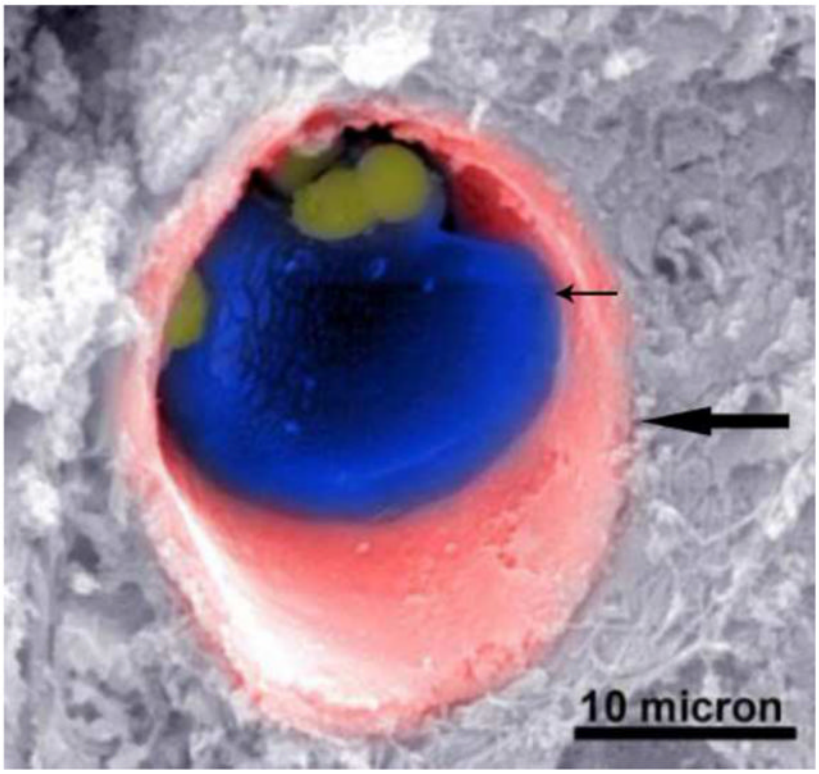

Figure 3.

(a) Hematoxylin and eosin–stained slide (180× magnification). MS are visualized as white spheres (black arrows) under light microscopy. **(b)** A scanning electron micrograph (3000× magnification) of a VX2 tumor shows the presence of MS (small arrow) in a tumor blood vessel (large arrow).

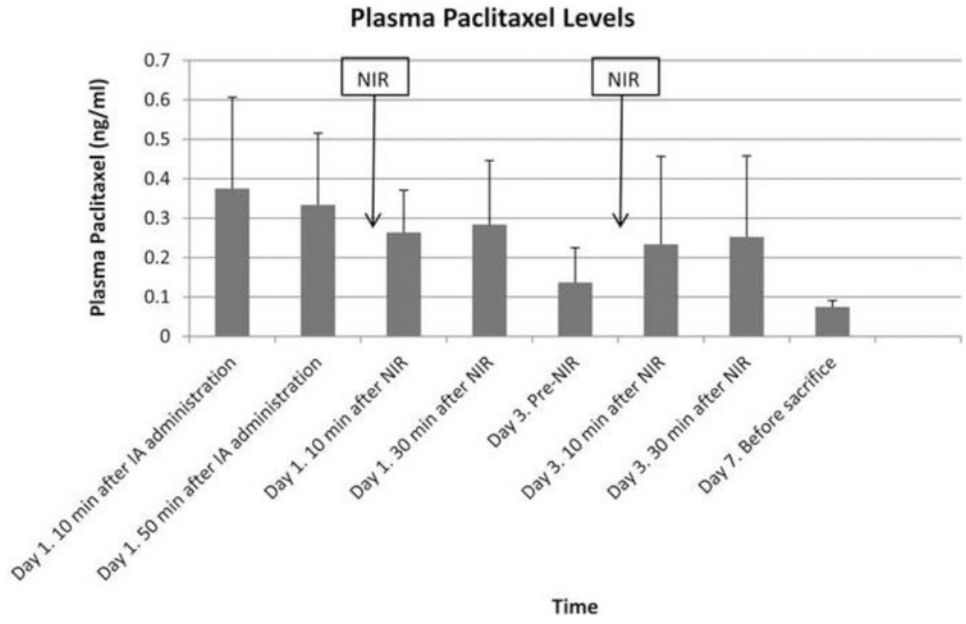

Figure 4.

Bar chart showing mean plasma PTX levels with 1 standard deviation error bars at different time points after IA administration of MS-HAuNS-PTX. The blood concentration of PTX was analyzed by using high-performance liquid chromatography.

Figure 5a

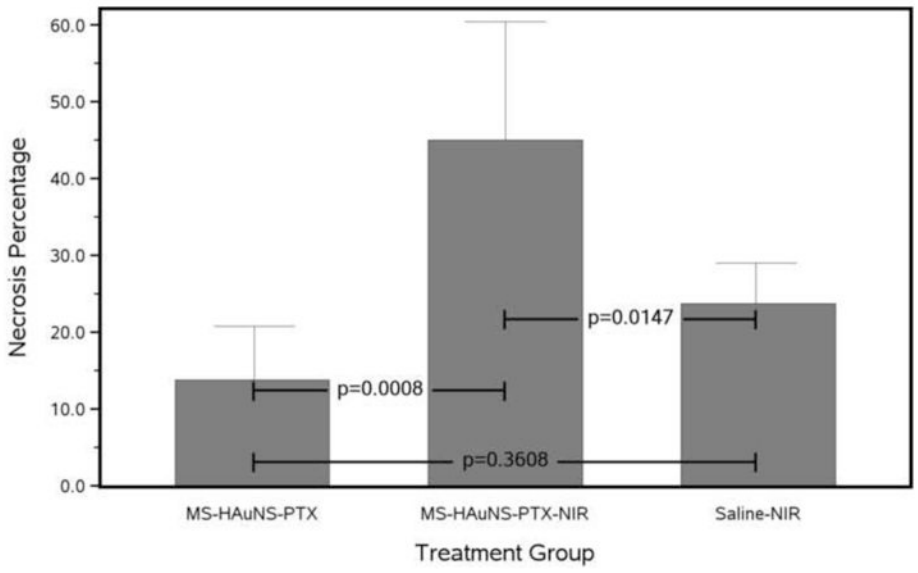

Figure 5b

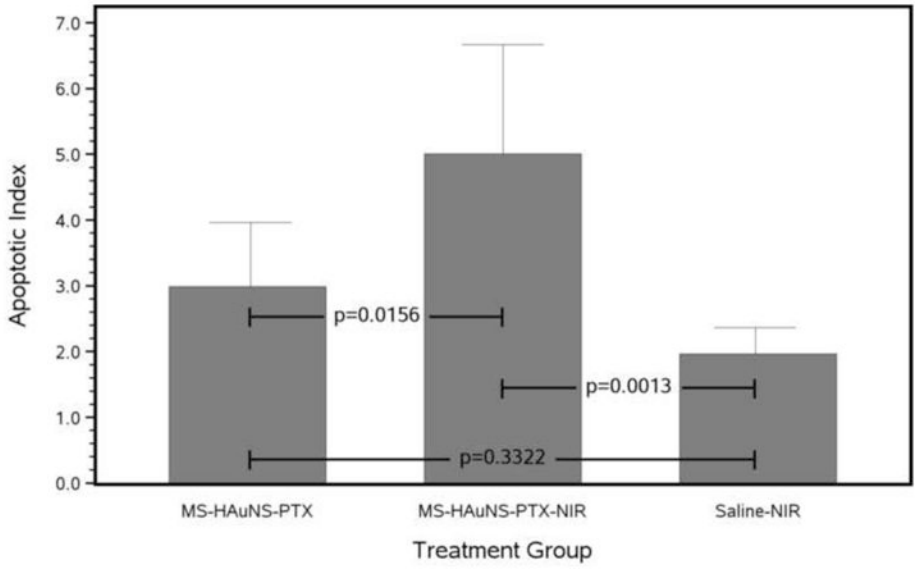

Figure 5.

Antitumor effects of various treatments on VX2 tumors grown in the liver of rabbits. **(a)** Bar chart of mean necrosis percentage for each treatment group with 1 standard deviation error bars and Tukey-Kramer adjusted pairwise *P* values. **(b)** Bar chart of mean apoptotic index for each treatment group with 1 standard deviation error bars and Tukey-Kramer adjusted pairwise *P* values.